ACS Catalysis

Letter

pubs.acs.org/acscatalysis

Synthesis and Catalytic Behavior of Ferrierite Zeolite Nanoneedles

Yoorim Lee,[†,§] Min Bum Park,[†,§] Pyung Soon Kim,[†] Aurélie Vicente,[‡] Christian Fernandez,[‡] In-Sik Nam,[†] and Suk Bong Hong[†,*]

[†]Department of Chemical Engineering and School of Environmental Science and Engineering, POSTECH, Pohang 790-784, Korea

[‡]Laboratoire Catalyse et Spectrochimie, ENSICAEN, Université de CAEN, CNRS, 6 Boulevard Maréchal Juin, 14050 CAEN, France

Supporting Information

ABSTRACT: The proton form of nanosized, needlelike ferrierite zeolite, which was synthesized using choline and Na^+ cations as structure-directing agents, was found to be much more efficient for the skeletal isomerization of 1-butene to isobutene than the corresponding cation form of conventional, submicrometric ferrierite with a platelike shape, mainly because of the considerably lower density of strong acid sites, but as well as a result of the higher density of 10-ring pore mouths.

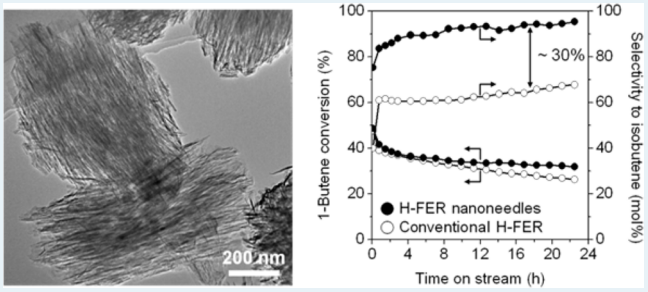

KEYWORDS: *ferrierite zeolite nanoneedles, synthesis, characterization, catalytic properties*

Zeolites are crystalline, microporous aluminosilicates whose applications as catalysts have led to an innovative shift in the petroleum and petrochemical industries due to the extreme uniformity in size and shape of their channels and cavities that enables shape-selective catalysis.[1,2] However, microporosity often brings about severe intracrystalline diffusion limitations, lowering the accessibility and molecular transport of reactive molecules to/from the active sites confined.[3] One way to solve this problem is to shorten the diffusion path length in zeolite micropores. Over the past decade, in fact, much attention has been devoted to the reduction of zeolite crystal size from the micrometric to the nanometric range. Consequently, more than 10 different structure types of nanocrystalline zeolites and phosphate-based molecular sieves have been successfully synthesized.[4−6]

Ferrierite (framework type FER) is a medium-pore, high-silica zeolite that contains a two-dimensional (2D) pore system consisting of 10-ring (4.2 × 5.4 Å) channels intersected by 8-ring (3.5 × 4.8 Å) channels.[7] This zeolite is well-known for the exceptional selectivity in the skeletal isomerization of *n*-butenes to isobutene.[8−12] Although ferrierite is a rare natural zeolite, it can also be synthesized using a variety of different organic structure-directing agents (SDAs) in the laboratory.[13] However, there is little known on the synthesis of nanosized ferrierite crystals. Here, we describe the synthesis of ferrierite nanoneedles with a Si/Al ratio of 9.9 using choline (Ch^+, (2-hydroxyethyl)trimethylammonium), one of the cheapest alkylammonium ions, and Na^+ as SDAs. We also report that the proton form (H-ferrierite) of this nanometric zeolite phase is much more selective and recyclable for the skeletal isomerization of 1-butene to isobutene than that of conventional, submicrometric ferrierite with a similar Si/Al ratio (8.9) but a different platelike crystal morphology.

Our interest in Ch^+ as an organic SDA began with the elegant work by Lewis and co-workers on the charge density mismatch synthesis of the large-pore zeolites UZM-4 (BPH) and UZM-22 (MEI) in the presence of this small organic cation together with Li^+, Sr^{2+}, or both.[14] Tetramethylammonium (TMA^+) and tetraethylammonium (TEA^+) ions, the two most studied organic SDAs in the synthesis of zeolites and molecular sieves, are slightly smaller and larger than Ch^+, respectively. Until now, at least 26 zeolitic materials with different framework topologies have been synthesized using one of TMA^+ and TEA^+, with or without inorganic cations present.[13] However, they include neither UZM-4 nor UZM-22, implying that Ch^+, although flexible due to its 2-hydroxyethyl chain, could be very selective for a particular zeolite structure once the right synthesis conditions are found. This stimulated us to investigate the influence of inorganic synthesis variables on the phase selectivity of the crystallization under the optimized conditions (ChOH/Si = 0.8 and Si/Al = 5) for UZM-4 formation.[14] As shown in Table 1, we were able to crystallize four different zeolitic phases, depending on the Al content of the synthesis mixtures and the concentration or type (or both) of alkali metal ions employed as a crystallization SDA.

When the crystallization was carried out under rotation (60 rpm) at 150 °C for 14 days, for example, ZSM-34, an intergrowth of offretite (OFF) and erionite (ERI),[15] was the product formed from a sodium aluminosilicate solution with Na/Si = 0.2 and Si/Al = 5. In addition, an increase in the Si/Al ratio of this synthesis solution to 20 resulted in the crystallization of ferrierite. When decreasing its Na/Si ratio to

Received: January 11, 2013
Revised: February 26, 2013
Published: February 27, 2013

Table 1. Representative Synthesis Conditions[a] and Results

run	M	Si/Al	product[b]	run	M	Si/Al	product[b]
1	Li^+	5	amorphous[c]	11	Li^+	20	ferrierite + RUB-10
2	Na^+	5	amorphous[c]	12	Na^+	20	ferrierite
3	K^+	5	ZSM-34	13	K^+	20	UZM-12
4	Rb^+	5	sodalite + U	14	Rb^+	20	amorphous[c]
5	Cs^+	5	PST-8 + amorphous + U	15	Cs^+	20	amorphous[c]
6	Li^+	10	ferrierite + RUB-10	16	Li^+	∞	amorphous[c]
7	Na^+	10	ferrierite + sodalite	17	Na^+	∞	PST-8
8	K^+	10	UZM-12 + U	18	K^+	∞	PST-8 + U
9	Rb^+	10	ferrierite + UZM-12	19	Rb^+	∞	PST-8 + U
10	Cs^+	10	ferrierite + sodalite	20	Cs^+	∞	amorphous[c]

[a]The oxide composition of the synthesis mixture is 4ChOH·MCl·xA-l_2O_3·5SiO_2·150H_2O, where M is Li^+, Na^+, K^+, Rb^+, or Cs^+ and x is 0, 0.125, 0.25, or 0.5, respectively. All the syntheses were performed under rotation (60 rpm) at 150 °C for 14 days unless otherwise stated. [b]The product appearing first is the major phase, and U indicates the unknown phase. [c]The material obtained after 28 days of heating.

0.1 (not shown in Table 1), however, we always obtained a small amount of RUB-10 (RUT) as an impurity phase, as well as ferrierite. On the other hand, the synthesis using an Al-free synthesis mixture with Na/Si = 0.2 yielded a layered silicate denoted PST-8. It is worth noting that while PST-8 is characterized by a powder X-ray diffraction (XRD) pattern that is quite similar to that of any of as-made ERS-12, PLS-1, MCM-65, UZM-13, etc.,[16−19] which are known to consist of ferrierite layers, its calcination in air at 550 °C led to a transformation into the CDO framework type material with poor crystallinity (Supporting Information Figure S1). This suggests that the ferrierite layers of PST-8 are stacked in a fairly less-ordered manner compared with those of layered materials with ferrierite layers described above. A structural investigation of PST-8 using synchrotron powder XRD data is in progress, and the results will be given elsewhere. Table 1 also shows that the replacement of NaCl with the equivalent amount of KCl under conditions where the formation of ferrierite proved to be reproducible gave UZM-12 (ERI), a high-silica analog of zeolite erionite.[20,21] It thus appears that the oxide composition range yielding pure ferrierite in the presence of ChOH is quite narrow.

Figure 1 shows the powder XRD pattern of the as-made ferrierite obtained from run 12 in Table 1. We note here that all the X-ray reflections are much broader than those observed for common ferrierite zeolite crystallized as the platelike morphology of a submicrometric scale (Supporting Information Figure S2), although their positions and relative intensities are in good agreement with each other, with the lack of a noticeable amorphous background. This suggests its nanocrystalline nature that can be further evidenced by the scanning and transition electron microscope images. As shown in Figure 1, our ferrierite appears as very small, heavily overlapped needles ∼10 nm in diameter and 100 nm in length, the lattice fringes of which are practically destroyed within a few seconds in the incident electron beam of 200 kV. In general, both natural and synthetic versions of ferrierite zeolite consist of

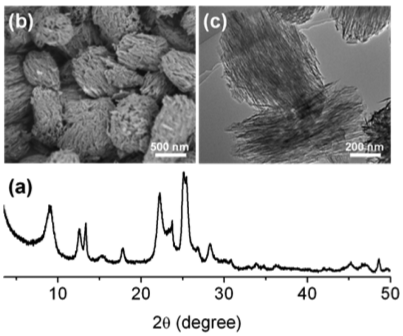

Figure 1. (a) Powder XRD pattern and (b) SEM and (c) TEM images of ferrierite nanoneedles synthesized in this work.

crystallites with a platelike morphology. However, the needle-like crystallites have also been reported in the literature.[22]

There is one patent shown in the literature on the Ch^+-mediated synthesis of a ferrierite-type zeolite designated ZSM-38, all the X-ray peaks of which are as broad as those observed for ferrierite zeolite described here, apart from the existence of two small impurity peaks around 2θ = 11.1 and 17.8° in its powder XRD pattern.[23] According to this patent, ZSM-38 can be obtained when a sodium aluminosilicate gel with Si/Al = 8.3 containing choline chloride (ChCl/Si = 0.16) and NaOH as SDAs is heated at 99 °C for 70 days or longer. Although the synthesis conditions of ZSM-38 are notably different from those of our ferrierite nanoneedles, most of its physicochemical properties, including the crystal morphology and size, are still unknown.

$^1H-^{13}C$ CP MAS NMR spectroscopy evidence that the Ch^+ ions are occluded mainly intact in ferrierite nanoneedles (Supporting Information Figure S3), and a combination of elemental and thermal analyses reveals that they have the unit cell composition $|Ch_{3.0}Na_{0.6}OH_{0.3}(H_2O)_{5.3}|$ $[Al_{3.3}Si_{32.7}O_{72}]$. Thus, there is an enrichment of Al in the product (Si/Al = 9.9) with respect to the synthesis mixture (Si/Al = 20). To further investigate the nanocrystalline nature of our ferrierite, we performed N_2 sorption measurements on its as-made and proton forms. Here, we outgassed as-made ferrierite at 150 °C under vacuum to a residual pressure of 10^{-5} Torr for 2 h before measurement to minimize the decomposition of the occluded Ch^+ ions. As shown in Figure 2, the isotherms of both materials are characterized by a hysteresis loop at high relative pressures, typical of mesoporosity: their external surface (or mesoporous) areas were determined to be ∼150 and 240 m^2 g^{-1}, respectively,

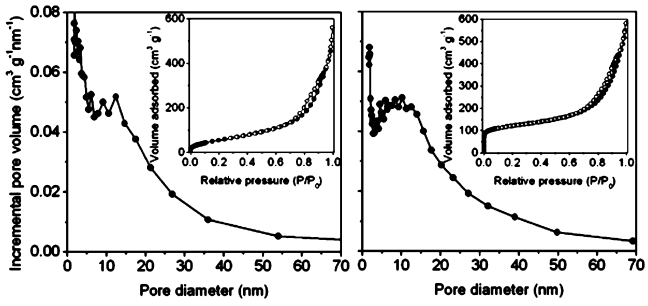

Figure 2. Pore size distribution curves for the as-made (left) and proton (right) forms of ferrierite nanoneedles calculated using the BJH formalism from the N_2 desorption branch isotherm. The inset shows the N_2 adsorption−desorption isotherms of the corresponding materials.

dx.doi.org/10.1021/cs400025s | ACS Catal. 2013, 3, 617−621

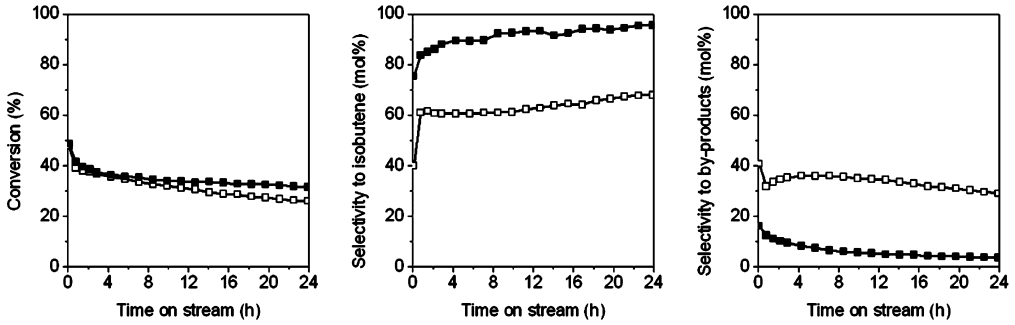

Figure 3. 1-Butene conversion (left), selectivity to isobutene (middle), and propene plus pentenes (right) as a function of time on stream in 1-butene skeletal isomerization at 400 °C and 10.1 kPa 1-butene pressure over H-FER(n) (■) and H-FER(c) (□).

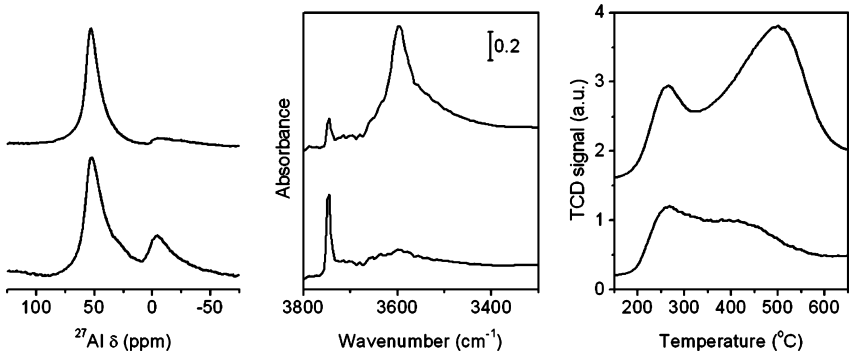

Figure 4. ^{27}Al MAS NMR spectra (left), IR spectra (middle) in the OH stretching region, and NH_3 TPD curves (right) of H-FER(n) (bottom) and H-FER(c) (top).

suggesting significant interparticle adsorption. Barrett–Joyner–Halenda (BJH) analyses indicate that they have an average pore size of ∼10 nm. From now on, for catalytic comparison, we will refer to our nanocrystalline ferrierite and a commercially available, submicrocrystalline ferrierite with a Si/Al ratio of 8.9 and a platelike shape of ∼0.7 μm in base and 0.1 μm in thickness (Supporting Information Figure S2) as FER(n) and FER(c), respectively.

Figure 3 shows 1-butene conversion and selectivity to isobutene and major byproducts as a function of time on stream (TOS) in the skeletal isomerization of 1-butene over H-FER(n) and H-FER(c) measured at 400 °C and 10.1 kPa 1-butene in the feed. It is well established that the rate of coke formation within the zeolite pores during this isomerization, which has a strong impact on the catalytic performance of zeolites, differs notably according to their acidic properties.[8−12] To minimize its effects on the isobutene selectivity, therefore, we regarded the results obtained at 5 min on stream as the intrinsic activities of these two H-FER catalysts with different morphologies and sizes. As shown in Figure 3, no large differences in the initial 1-butene conversion are observed. However, notice that the initial isobutene selectivity (75%) of nanocrystalline H-FER(n) is much higher than that (40%) of submicrocrystalline H-FER(c). A similar trend can also be observed over the period of TOS studied, although the extent of selectivity increase with TOS was greater for the latter catalyst, making the selectivity difference (∼30%) slightly smaller.

Although much controversy remains on the reaction mechanism by which isobutene is produced over H-FER in the steady state, there is a general acceptance that the initial isobutene formation is dominated by the nonselective bimolecular mechanism, that is, dimerization followed by cracking.[12] The ^{27}Al MAS NMR spectrum of as-made FER(n), as well as that of the parent NaK form of FER(c), exhibits only one resonance around 50 ppm (Supporting Information Figure S4), typical of tetrahedral Al in the zeolite framework. As shown in Figure 4, however, the ^{27}Al MAS NMR spectra of H-FER(n) and H-FER(c) are characterized by an additional resonance around 0 ppm. Because the relative intensity (∼29 vs 14%) of this ^{27}Al resonance is considerably stronger in the spectrum of H-FER(n) than in that of H-FER(c), it is clear that the amount of Al atoms extracted from the zeolite framework during the preparation of their proton form is much higher for the nanocrystalline zeolite, although there is no detectable decrease in X-ray peak intensity. When combining with data from elemental analysis, the framework Si/Al ratios of H-FER(n) and H-FER(c) were determined to be 13.9 and 10.3, respectively. Quite similar ratios (13.6 and 10.1) were also derived from the deconvolution of their ^{29}Si MAS NMR spectra (Supporting Information Figure S5).

The point given above can be further supported by the IR and NH_3 temperature-programmed desorption (TPD) results (Figure 4). The intensity of the IR band around 3600 cm^{-1} due to the hydroxyl groups of Brønsted acid sites was found to be much weaker for H-FER(n) than for H-FER(c). In addition, deconvolution of the NH_3 TPD curves shows that the total area of NH_3 desorption (i.e., the density of acid sites) of H-FER(n) is about 40% that of H-FER(c). In particular, the area of the high-temperature desorption peak around 500 °C due to strong acid sites, which induce undesired side reactions such as dimerization followed by cracking into byproducts such as propene and pentenes during 1-butene skeletal isomerization,[12] from the former catalyst was found to be only one-fourth that from the latter one. This explains why H-FER(n) gives a higher initial isobutene selectivity than H-FER(c), together with a fairly low selectivity to byproducts (Figure 3).

dx.doi.org/10.1021/cs400025s | ACS Catal. 2013, 3, 617−621

On the other hand, the spatial distribution of Al atoms (i.e., Brønsted acid sites) in the zeolite framework can be altered by the size and charge distribution of organic SDAs employed.[19,24,25] To examine differences in the location of acid sites in H-FER(n) and H-FER(c), we collected their ^{27}Al 3QMAS NMR spectra (Supporting Information Figure S6). Although H-FER(n) has a higher amount of Al in the extraframework environment than H-FER(c), no significant differences in the shape of the tetrahedral ^{27}Al resonance were found. This suggests that notable differences in their acidic properties have no relation with the framework Al distribution. A recent study by Kim et al.[26] has shown that the acid sites on the external surface of nanocrystalline ZSM-5 zeolites, whose density should be inversely proportional to the crystal size, are weaker in acid strength than those in their intracrystalline space. It thus appears that nanocrystallinity could also exert a great influence on the acidity of H-FER zeolites. However, the details are unclear at this time.

The 3QMAS NMR results also suggest that a quite similar consideration could be made for the dealumination behavior of zeolites. However, the actual situation is not so simple, because H-NU-88 (Si/Al ∼ 13), a nanocrystalline material with a crystallite size of 20−30 nm that could be an intergrowth of several hypothetical polymorphs in the beta family of zeolites, has no detectable extraframework Al species, even after heating at 800 °C.[27] This led us to suspect that the structural feature of zeolites may have a greater effect on the extent of dealumination than their nanocrystallinity.

The 10-ring channels of the FER framework structure are reported to be perpendicular to the (001) surface of the platelike FER crystals that are thus parallel to their basal lines (Supporting Information Figure S7).[12,28] Assuming that they are along with the long axis of needlelike FER(n) crystallites with 10 nm in mean diameter and 100 nm in mean length, the number of the 10-ring channels at their boundary (i.e., 10-ring pore mouths) was calculated to be about 9 times larger than that of the analogous mouths of the equivalent weight of platelike H-FER(c) crystals with ∼0.7 μm base and 0.1 μm thickness. This ratio is more than twice as large as that (4) of their external surface areas (240 vs 60 $m^2\ g^{-1}$) derived from the t-plot method, which appears to originate from the heavily overlapped nature of our FER nanoneedles, as well as from the assumption of cylindrical geometry. However, it is clear that the number of Brønsted acid sites at or near the 10-ring pore mouths should be much larger on H-FER(n) than on H-FER(c), although the former zeolite has a somewhat higher framework Si/Al ratio (∼14 vs 10).

According to the knowledge accumulated thus far, there are two major types of prevailing reaction mechanisms in the selective formation of isobutene over H-FER zeolite after some TOS: (i) the pseudomonomolecular pathway involving an alkylaromatic tertiary carbenium ion and (ii) the monomolecular pathway involving a primary carbenium ion.[12] A combination of thermogravimetric and differential thermal analyses (TGA/DTA) reveals that the amount of (5.5 vs 9.1 wt %) of coke deposited during the 1-butene skeletal isomerization at 400 °C for 24 h is considerably smaller in H-FER(n) than in H-FER(c) (Supporting Information Figure S8), which can be further supported by ex situ gas chromatography−mass spectroscopy (Supporting Information Figure S9). Despite notable differences in their acidity, in addition, the main components (bi- and tricyclic aromatic species) of their coke deposits were found to be essentially identical with each other.

Thus, if the pseudomonomolecular mechanism is prevailing with prolonged TOS, the number of highly selective sites for isobutene formation, that is, alkylaromatic tertiary carbenium ions on the coke molecules located near the zeolite pore mouths,[11,29] should then be larger for H-FER(c) with a higher coke content. As shown in Figure 3, however, a considerably higher isobutene selectivity after some TOS is observed for H-FER(n) with a lower coke content. As previously proposed by our group,[28] therefore, it appears that 1-butene skeletal isomerization over aged H-FER takes place over the Brønsted acid sites located at or near its 10-ring pore mouths, although this monomolecular mechanism cannot avoid the energetically unfavorable ring-opening of a cyclopropyl cation. We also note that H-FER(n) shows better recyclability in this reaction than H-FER(c). As can be found in Supporting Information Figure S10, the extent of decrease in 1-butene conversion and isobutene selectivity at 12 h on stream during the four successive catalytic cycles carried out at 400 °C for 24 h was lower for the former catalyst. This is not unexpected because nanocrystallinity leads to shorter diffusion path in zeolite micropores and is thus of great advantage to regenerate used zeolite catalysts upon calcination in flowing air at elevated temperatures.

In summary, we have successfully synthesized ferrierite zeolite nanoneedles with a Si/Al ratio of 9.9 using choline and Na^+ ions as SDAs. We also found that the proton form of this nanocrystalline zeolite is a considerably more efficient catalyst for the skeletal isomerization of 1-butene to isobutene than the corresponding cation form of conventional, submicrometric H-ferrierite with a similar bulk Si/Al ratio (8.9) but a different platelike crystal morphology. The overall results of our work suggest that monomolecular, pore mouth shape catalysis over the Brønsted acid sites located at or near the 10-ring pore mouths is the origin of the remarkable isobutene selectivity of H-ferrierite observed only after some time on stream.

■ ASSOCIATED CONTENT

Ⓢ Supporting Information

Details of experimental procedures, powder XRD, ^{1}H−^{13}C CP, ^{27}Al, and ^{29}Si MAS and ^{27}Al 3QMAS NMR, crystal morphology illustrations, TGA/DTA, GC-MS, and results of recyclability test. This material is available free of charge via the Internet at http://pubs.acs.org/.

■ AUTHOR INFORMATION

Corresponding Author

*E-mail: sbhong@postech.ac.kr.

Author Contributions

§These authors contributed equally.

Notes

The authors declare no competing financial interest.

■ ACKNOWLEDGMENTS

This work was supported by the National Research Foundation (2012R1A3A2048833, 2012K1A3A4A07030457, and 2012-0008674) of Korea and by the Pierre Hubert Curien STAR program (2012 Project No. 27816PB) of France.

■ REFERENCES

(1) Degnan, T. F. *J. Catal.* **2003**, *216*, 32.
(2) Camblor, M. A.; Hong, S. B. In *Porous Materials*; Bruce, D. W., Walton, R. L., O'Hare, D., Eds.; Wiley: Chichester, 2011; p 265.

(3) Pérez-Ramírez, J.; Christensen, C. H.; Egeblad, K.; Christensen, C. H.; Groen, J. C. *Chem. Soc. Rev.* **2008**, *37*, 2530.
(4) Tosheva, L.; Valtchev, V. P. *Chem. Mater.* **2005**, *17*, 2494.
(5) Ng, E.-P.; Chateigner, D.; Bein, T.; Valtchev, V.; Mintova, S. *Science* **2012**, *335*, 70.
(6) Zhang, X.; Liu, D.; Xu, D.; Asahina, S.; Cychosz, K. A.; Agrawal, K. V.; Al Wahedi, Y.; Bhan, A.; Al Hashimi, S.; Terasaki, O.; Thommes, M.; Tsapatsis, M. *Science* **2012**, *336*, 1684.
(7) Baerlocher, Ch.; McCusker, L. B. Database of Zeolite Structures; http://www.iza-structure.org/databases/ (Accessed March 2, 2013)..
(8) Mooiweer, H. H.; de Jong, K. P.; Kraushaar-Czarnetzki, B.; Storkk, W. H. J.; Krutzen, B. C. H. *Stud. Surf. Sci. Catal.* **1994**, *84*, 2327.
(9) O'Young, C.-L.; Pellet, R. J.; Casey, D. G.; Ugolini, J. R.; Sawicki, R. A. *J. Catal.* **1995**, *151*, 467.
(10) Seo, G.; Jeong, H. S.; Jang, D.-L.; Cho, D. L.; Hong, S. B. *Catal. Lett.* **1996**, *41*, 189.
(11) Guisnet, M.; Andy, P.; Gnep, N. S.; Travers, C.; Benazzi, E. *J. Chem. Soc., Chem. Commun.* **1995**, 1685.
(12) van Donk, S.; Bitter, J. H.; de Jong, K. P. *Appl. Catal., A* **2001**, *212*, 97.
(13) Szostak, R. *Handbook of Molecular Sieves*; Van Nostrand Reinhold: New York, 1992.
(14) Miller, M. A.; Moscoso, J. G.; Koster, S. C.; Gatter, M. G.; Lewis, G. J. *Stud. Surf. Sci. Catal.* **2007**, *170A*, 347.
(15) Rubin, M. K.; Rosinski, E. J.; Plank, C. J. U.S. Patent 4,086,186, 1978.
(16) Ikeda, T.; Akiyama, Y.; Oumi, Y.; Kawai, A.; Mizukami, F. *Angew. Chem., Int. Ed.* **2004**, *43*, 4892.
(17) Millini, R.; Carluccio, L. C.; Carati, A.; Bellussi, G.; Perego, C.; Cruciani, G.; Zanardi, S. *Microporous Mesoporous Mater.* **2004**, *74*, 59.
(18) Dorset, D. L.; Kennedy, G. J. *J. Phys. Chem. B* **2004**, *108*, 15216.
(19) Knight, L. M.; Miller, M. A.; Koster, S. C.; Gatter, M. G.; Benin, A. I.; Wills, R. R.; Lewis, G. J.; Broach, R. W. *Stud. Surf. Sci. Catal.* **2007**, *170A*, 338.
(20) Miller, M. A.; Lewis, G. J.; Moscoso, J. G.; Koster, S.; Modica, F.; Gatter, M. G.; Nemeth, L. T. *Stud. Surf. Sci. Catal.* **2007**, *170A*, 487.
(21) Lee, J. H.; Park, M. B.; Lee, J. K.; Min, H.-K.; Song, M. K.; Hong, S. B. *J. Am. Chem. Soc.* **2010**, *132*, 12971.
(22) Pinar, A. B.; Gomez-Hortiguela, L.; Perez-Pariente, J. *Chem. Mater.* **2007**, *19*, 5617.
(23) Plank, C. J.; Rosinski, E. J.; Rubin, M. K. U.S. Patent 4,046,859, 1977.
(24) Shantz, D. F.; Lobo, R. F. *J. Phys. Chem. B* **1998**, *102*, 2339.
(25) Shantz, D. F.; Lobo, R. F. *Chem. Mater.* **1998**, *10*, 4015.
(26) Kim, K.; Ryoo, R.; Jang, H.-D.; Choi, M. *J. Catal.* **2012**, *288*, 115.
(27) Lee, S.-H.; Lee, D.-K.; Shin, C.-H.; Park, Y.-K.; Wright, P. A.; Lee, W. M.; Hong, S. B. *J. Catal.* **2003**, *215*, 151.
(28) Lee, S.-H.; Shin, C.-H.; Hong, S. B. *J. Catal.* **2004**, *223*, 200.
(29) Andy, P.; Gnep, N. S.; Guisnet, M.; Benazzi, E.; Travers, C. *J. Catal.* **1998**, *173*, 322.